Computers and Fluids 227 (2021) 105021

Contents lists available at ScienceDirect

Computers and Fluids

journal homepage: www.elsevier.com/locate/compfluid

A simple FORCE-type centred scheme accurate for contact discontinuities: Application to compressible Euler flows

Lijun Hu[a,*], Li Yuan[b,c]

[a] School of Mathematics and Statistics, Hengyang Normal University, Hengyang, Hunan 421002, China
[b] ICMSEC and LSEC, Academy of Mathematics and Systems Science, Chinese Academy of Sciences, Beijing 100190, China
[c] School of Mathematical Sciences, University of Chinese Academy of Sciences, Beijing 100190, China

ARTICLE INFO

Article history:
Received 24 September 2020
Revised 15 April 2021
Accepted 26 May 2021
Available online 31 May 2021

Keywords:
Euler equations
Centred schemes
FORCE scheme
Contact discontinuity
Carbuncle phenomenon
Boundary variation diminishing

ABSTRACT

The FORCE-type centred schemes are simple and efficient and do not explicitly require the wave propagation information of the system to calculate the numerical flux. However, their poor resolution for contact discontinuities seriously affects their applications. In the present work, a simple FORCE-type centred scheme accurate for contact discontinuities is proposed and applied to calculations of compressible Euler flows. The missing contact wave of the original FORCE centred scheme is restored with an algebraic method and the resolution for contact discontinuities is further improved by using the boundary variation diminishing (BVD) algorithm to minimize the density jump in the numerical diffusion term of the original FORCE centred scheme. Numerical results of several one- and two-dimensional benchmark test problems fully demonstrate that the proposed centred scheme is capable of capturing contact discontinuities more sharply than the complete-wave HLLC upwind scheme. In addition, another advantage of the proposed centred scheme is that it is free from the carbuncle phenomenon which afflicts many contact-capturing upwind schemes (e.g. Roe and HLLC) in calculations of multidimensional flow problems involving strong shock waves.

1. Introduction

Numerical fluxes at cell interfaces are the building block for solving the hyperbolic conservation laws numerically in the framework of finite volume method and thus the construction of monotone numerical fluxes has been a central research issue in the field of computational fluid dynamics over the past few decades [1]. Upwind and centred schemes are two representative numerical methods to obtain the numerical flux through a cell interface. Generally, the upwind schemes require to explicitly provide the wave information propagating along the direction orthogonal to a cell interface, which is usually achieved via the solution of a local one-dimensional Riemann problem involving two constant states [2]. In many cases, it is either unavailable or computationally expensive to obtain the exact solution of a Riemann problem. Therefore the construction of a reliable approximate Riemann solver is the key to a successful upwind scheme. In the past few decades, researchers had developed a number of approximate Riemann solvers that can be applied to solve different flow problems and they are usually classified as complete-wave solvers and incomplete-wave solvers according to their capabilities of resolving contact discontinuities and shear waves. The incomplete-wave solvers, such as the HLL scheme [3], HLLE scheme [4] and HLL-CPS scheme [5], omit one or both of these waves due to their high numerical dissipation behaviours and thus they are not the appropriate choices in calculations of flow problems involving the shear-dominated phenomenon, vortex, material interface, mixing layer, etc [6]. The complete-wave solvers, such as the Roe's scheme [7], Osher's scheme [8], HLLEM scheme [9] and HLLC scheme [10], are capable of capturing the contact discontinuities and shear waves accurately in calculations. However, the severe carbuncle instability occurring near the multidimensional strong shock waves will afflict them and badly affect their accurate simulations for high Mach flow problems.

Different from the upwind schemes that heavily rely on the eigen-structure (eigenvalues and eigenvectors) of the system to calculate the numerical flux, there is no explicit requirement for the wave propagation information in the centred schemes except the maximum eigenvalue of the system which is required for the stability CFL condition. In the framework of the centred schemes, although the initial conditions constitute a local Riemann problem, the data is updated by integrating the controlling equations on two sets of meshes, i.e. the primary mesh and staggered mesh, rather

* Corresponding author.
E-mail addresses: hulijun@lsec.cc.ac.cn (L. Hu), lyuan@lsec.cc.ac.cn (L. Yuan).

https://doi.org/10.1016/j.compfluid.2021.105021
0045-7930/

than explicitly solving the Riemann problem. In other words, although the centred schemes are not completely independent of the Riemann problem they solve it in an unconventional approach that is radically different from the one the upwind schemes take [1]. Therefore, for numerically solving those overly complex systems for which the solution of the Riemann problem is not easy to obtain, the centred schemes are appropriate choices. Early representatives of the centred schemes are the Lax-Friedrichs scheme [11] and Nessyahu-Tadmor scheme [12] for one-dimensional cases. In the last decades, many researchers were devoted to extending the original Lax-Friedrichs and Nessyahu-Tadmor centred schemes to multidimensional unstructured meshes and high-order accuracy, e.g. see [13–16].

Recently, Toro and Billett [17] constructed a one-dimensional first order centred (FORCE) scheme and the extension to the multidimensional hyperbolic systems of conservation laws on unstructured meshes had been proposed in [1]. Dumbser et al. [18] developed a FORCE centred scheme on unstructured meshes for solving the non-conservative hyperbolic systems and a version on the moving unstructured meshes for both the conservative and non-conservative hyperbolic systems was proposed by Boscheri et al. [19]. The FORCE centred scheme is monotone and has an optimal stability CFL restriction of unity. In addition, it can be recast into a one-step procedure on a non-staggered mesh and has a conservative form whose numerical flux just involves the left and right states of the cell interface. Therefore the high-order accuracy of the scheme is easily achieved through the existing reconstruction techniques and it can also be incorporated into the finite volume or DG finite element methods straightforwardly [20]. However, due to no consideration of the wave structures of the system, the centred schemes, of course including the FORCE scheme, tend to be more dissipative than the upwind schemes, especially for the contact discontinuity corresponding to the linearly degenerate field. In order to improve the capability of the centred schemes to capture contact waves, Kurganov and Lin [21] constructed a semi-discrete centred scheme and an upwind-biased FORCE scheme (UFORCE) with applications to shallow-water equations was proposed by Stecca et al. [22]. Canestrelli and Toro [20,23] proposed a FORCE-type centred scheme with restoration of contact surfaces to solve the conservative and non-conservative shallow water equations.

In the present work, a contact-capturing FORCE-type centred scheme with applications to compressible Euler flows is proposed. The missing contact wave of the original FORCE scheme is restored with an algebraic method and the boundary variation diminishing (BVD) algorithm [24] is used to further improve the resolution of the proposed scheme for contact discontinuities. Compared with the complete-wave HLLC upwind scheme, the proposed scheme has higher resolution for contact discontinuities and better robustness against the shock anomalies. In addition, numerical results also confirm that the proposed scheme has better contact capturing ability than the robust TV flux splitting scheme in [25]. The paper is organised as follows. Section 2 gives some preliminaries. In Section 3, the construction of a contact-capturing FORCE-type centred scheme is described in detail. Section 4 presents the numerical results of several benchmark test problems to demonstrate the accuracy and robustness of the proposed scheme. A brief conclusion is given in Section 5.

2. Background

Consider the two-dimensional inviscid Euler equations

$$\frac{\partial \mathbf{U}}{\partial t}+\frac{\partial \mathbf{F}(\mathbf{U})}{\partial x}+\frac{\partial \mathbf{G}(\mathbf{U})}{\partial y}=\mathbf{0}, \tag{2.1}$$

where the vector of conserved variables $\mathbf{U}$, the fluxes in both directions $\mathbf{F}(\mathbf{U})$ and $\mathbf{G}(\mathbf{U})$ are given by

$$\mathbf{U}=\begin{bmatrix}\rho\\ \rho u\\ \rho v\\ E\end{bmatrix},\quad \mathbf{F}(\mathbf{U})=\begin{bmatrix}\rho u\\ \rho u^2+p\\ \rho uv\\ u(E+p)\end{bmatrix},\quad \mathbf{G}(\mathbf{U})=\begin{bmatrix}\rho v\\ \rho uv\\ \rho v^2+p\\ v(E+p)\end{bmatrix}. \tag{2.2}$$

Here ρ is the density, u and v are velocity components in the x- and y-directions, p is the pressure and E is the total energy. System (2.1) is closed through the following equation of state

$$p=(\gamma-1)\left[E-\frac{1}{2}\rho\left(u^2+v^2\right)\right], \tag{2.3}$$

where γ is the specific heat ratio.

2.1. Finite volume method

The integral form of system (2.1) can be written as

$$\frac{d}{dt}\int_{\Omega}\mathbf{U}d\Omega+\oint_{\partial\Omega}[(\mathbf{F},\mathbf{G})\cdot\mathbf{n}]dl=\mathbf{0}, \tag{2.4}$$

where $\partial\Omega$ is the boundary of the control volume Ω, $\mathbf{n}$ denotes the outward unit vector normal to the line element dl.

We discretize system (2.4) with the finite volume method over a 2D domain covered by structured quadrilateral cells. The semi-discrete equations over a specific control volume $\Omega_{i,j}$ can be written as

$$\frac{d\mathbf{U}_{i,j}}{dt}=-\frac{1}{|\Omega_{i,j}|}\sum_{k=1}^{4}[(\mathbf{F},\mathbf{G})_k\cdot\mathbf{n}_k]\Delta l_k, \tag{2.5}$$

where $\mathbf{U}_{i,j}$ is the cell-average of $\mathbf{U}$ on $\Omega_{i,j}$ and $|\Omega_{i,j}|$ is the volume of $\Omega_{i,j}$, Δl_k denotes the length of the cell interface I_k and $\mathbf{n}_k$ is the outward unit vector normal to I_k. Using the rotational invariance property of two-dimensional Euler equations, the numerical flux $(\mathbf{F},\mathbf{G})_k\cdot\mathbf{n}_k$ through the cell interface I_k can be written as

$$(\mathbf{F},\mathbf{G})_k\cdot\mathbf{n}_k=\mathbf{T}_k^{-1}\mathbf{F}(\mathbf{T}_k\mathbf{U}_L,\mathbf{T}_k\mathbf{U}_R), \tag{2.6}$$

where $\mathbf{T}_k$ and $\mathbf{T}_k^{-1}$ denote the rotation matrices.

2.2. FORCE scheme

The conservative form of the numerical flux of the first order centred (FORCE) scheme [1] can be expressed as

$$\overline{\mathbf{F}}^{\mathrm{FORCE}}_{i+1/2,j}=\frac{1}{2}\left[\mathbf{F}(\mathbf{U}_{i+1/2,j})+\frac{1}{2}(\mathbf{F}(\mathbf{U}_L)+\mathbf{F}(\mathbf{U}_R))-\frac{1}{4}\frac{\Delta x}{\Delta t}(\mathbf{U}_R-\mathbf{U}_L)\right], \tag{2.7}$$

with

$$\mathbf{U}_{i+1/2,j}=\frac{1}{2}(\mathbf{U}_L+\mathbf{U}_R)-\frac{1}{2}\left(\frac{2\Delta t}{\Delta x}\right)[\mathbf{F}(\mathbf{U}_R)-\mathbf{F}(\mathbf{U}_L)]. \tag{2.8}$$

The FORCE flux given by (2.7) can be rewritten as the arithmetic average of the Lax-Wendroff flux and the Lax-Friedrichs flux

$$\overline{\mathbf{F}}^{\mathrm{FORCE}}_{i+1/2,j}=\frac{1}{2}\left(\overline{\mathbf{F}}^{\mathrm{LW}}_{i+1/2,j}+\overline{\mathbf{F}}^{\mathrm{LF}}_{i+1/2,j}\right), \tag{2.9}$$

where

$$\overline{\mathbf{F}}^{\mathrm{LW}}_{i+1/2,j}=\mathbf{F}(\mathbf{U}_{i+1/2,j}) \tag{2.10}$$

and

$$\overline{\mathbf{F}}^{\mathrm{LF}}_{i+1/2,j}=\frac{1}{2}[\mathbf{F}(\mathbf{U}_L)+\mathbf{F}(\mathbf{U}_R)]-\frac{1}{2}\left(\frac{\Delta x}{2\Delta t}\right)(\mathbf{U}_R-\mathbf{U}_L). \tag{2.11}$$

3. A FORCE-type flux accurate for contact discontinuities

The FORCE flux given by (2.7) is monotone and has a optimal stability CFL restriction of unity. However, the resolution for contact discontinuities is extremely unsatisfactory due to its inherent dissipation behaviour. On the other hand, thanks to the inherent numerical dissipation, the FORCE flux is very robust in calculations of flow problems involving strong shock waves. In what follows, we propose a simple strategy to restore the missing contact discontinuity of the FORCE flux while preserving its robustness against shock anomalies.

3.1. FORCE-BVD scheme

The FORCE flux given by (2.7) consists of two parts, i.e. the Lax-Wendroff flux capable of capturing the isolated stationary contact discontinuity exactly and the dissipative Lax-Friedrichs flux. Thus the reduction of numerical dissipation inherent in the Lax-Friedrichs flux can greatly improve the resolution of the FORCE centred scheme for contact discontinuities. The Lax-Friedrichs flux given by (2.11) can be rewritten as

$$\overline{\mathbf{F}}^{\mathrm{LF}}_{i+1/2,j} = \frac{1}{2}[\mathbf{F}(\mathbf{U}_L) + \mathbf{F}(\mathbf{U}_R)] + \mathbf{D}_{1/2}, \tag{3.1}$$

with

$$\mathbf{D}_{1/2} = -\frac{1}{2}\left(\frac{\Delta x}{2\Delta t}\right)\begin{bmatrix} \rho_R - \rho_L \\ (\rho u)_R - (\rho u)_L \\ (\rho v)_R - (\rho v)_L \\ E_R - E_L \end{bmatrix}, \tag{3.2}$$

where the first term on the right hand side of (3.1) is the central difference term and $\mathbf{D}_{1/2}$ corresponds to a numerical dissipation term.

Specifically, the excessive numerical dissipation due to the density jump $|\rho_R - \rho_L|$ in $\mathbf{D}_{1/2}$ causes the failure of the FORCE scheme to capture contact discontinuities [5]. In the present work, we propose a simple strategy to minimize the density jump $|\rho_R - \rho_L|$ and thus to reduce the contribution of the dissipation term $\mathbf{D}_{1/2}$ to the numerical flux. Following ideas proposed in [24,26,27], we use the THINC (Tangent of Hyperbola for INterface Capturing) reconstruction [28] to obtain the density values

$$\rho_i(x) = \rho_{\min} + \frac{\Delta\rho}{2}\left[1 + \theta\tanh\left(\beta\left(\frac{x - x_{i-1/2}}{x_{i+1/2} - x_{i-1/2}} - \tilde{x}_i\right)\right)\right], \tag{3.3}$$

where $\rho_{\min} = \min(\rho_{i-1}, \rho_{i+1})$, $\Delta\rho = |\rho_{i+1} - \rho_{i-1}|$, $\theta = \mathrm{sgn}(\rho_{i+1} - \rho_{i-1})$ and β is a parameter to control the jump thickness. A larger β will give a solution with less dissipation while a smaller one tends to produce a solution with more dissipation. The value of β ranging from 1.2 to 2.0 is capable of giving a satisfactory solution and it is taken as 1.6 in the present work.

The unknown $\tilde{x}_i$ is the position of the jump center, which is calculated from the constraint condition, $\rho_i = \frac{1}{\Delta x}\int_{x_{i-1/2}}^{x_{i+1/2}} \rho_i(x)dx$. For convenience, we give explicitly the formula to calculate the reconstructed density values on the left and right sides of the cell interface [24],

$$\begin{aligned} \rho_i(x_{i+1/2}) &= \rho_{\min} + \tfrac{\Delta\rho}{2}\left[1 + \theta\tfrac{\tanh(\beta)+A}{1+A\tanh(\beta)}\right], \\ \rho_i(x_{i-1/2}) &= \rho_{\min} + \tfrac{\Delta\rho}{2}(1 + \theta A), \end{aligned} \tag{3.4}$$

where

$$A = \frac{B - \cosh(\beta)}{\sinh(\beta)}, \quad B = \exp\left[\theta\beta\left(2\frac{\rho_i - \rho_{\min} + \varepsilon}{\Delta\rho + \varepsilon} - 1\right)\right], \quad \varepsilon = 10^{-20}. \tag{3.5}$$

Having finished the THINC reconstruction procedure (3.4) in each cell, we can obtain the density values $\rho^{\mathrm{T}}_{L/R}$ (subscript 'T' stands for the THINC reconstruction) on both sides of each cell interface. On the other hand, we can use the polynomial reconstruction to obtain the density values $\rho^{\mathrm{P}}_{L/R}$ (subscript 'P' stands for the polynomial reconstruction) on both sides of each cell interface. In the present work, the MUSCL reconstruction procedure [29] is implemented to obtain the density values $\rho^{\mathrm{P}}_{L/R}$.

In order to further improve the resolution of the proposed scheme for contact discontinuities, the BVD algorithm [24,27] is implemented to minimize the density jump $|\rho_R - \rho_L|$ across the cell interface

$$|\rho_R - \rho_L| = \min(|\rho^{\mathrm{T}}_R - \rho^{\mathrm{T}}_L|,\ |\rho^{\mathrm{P}}_R - \rho^{\mathrm{P}}_L|,\ |\rho^{\mathrm{T}}_R - \rho^{\mathrm{P}}_L|,\ |\rho^{\mathrm{P}}_R - \rho^{\mathrm{T}}_L|). \tag{3.6}$$

The final density values $\rho_{L/R}$ on both sides of the cell interface in $\mathbf{D}_{1/2}$ can be determined by (3.6) and the numerical dissipation term $\mathbf{D}_{1/2}$ can now be rewritten as

$$\mathbf{D}_{1/2} = -\frac{1}{2}\left(\frac{\Delta x}{2\Delta t}\right)\begin{bmatrix} \rho_R - \rho_L \\ \rho_R u_R - \rho_L u_L \\ \rho_R v_R - \rho_L v_L \\ \left(\frac{p_R}{\gamma-1} + \frac{1}{2}\rho_R(u_R^2 + v_R^2)\right) - \left(\frac{p_L}{\gamma-1} + \frac{1}{2}\rho_L(u_L^2 + v_L^2)\right) \end{bmatrix}. \tag{3.7}$$

To summarize, the numerical flux of the FORCE-type centred scheme with Boundary Variation Diminishing (named as FORCE-BVD) is obtained by the following four steps:

1. Calculate the density values $\rho^{\mathrm{P}}_{L/R}$ on both sides of the cell interface with the MUSCL scheme or other higher-order polynomial reconstruction methods, e.g. WENO reconstruction;
2. Calculate the density values $\rho^{\mathrm{T}}_{L/R}$ with the THINC reconstruction given by (3.4) to restore the discontinuous density field;
3. Determine the final density values $\rho_{L/R}$ with the BVD algorithm (3.6) to minimize the density jump in the numerical dissipation term $\mathbf{D}_{1/2}$ and thus to resolve the contact discontinuities more sharply;
4. The final numerical flux of the proposed FORCE-BVD centred scheme is obtained through (2.8)-(2.10), (3.1) and (3.7).

In the present work, the multidimensional computation is conducted by the operator splitting method and the THINC reconstruction is carried out in a dimension-by-dimension fashion. Thus the one-dimensional building block presented above can be used straightforwardly in each coordinate direction in multidimensional computation. As an algebraic method, the THINC reconstruction does not involve any geometric reconstruction in multidimensional implementation, but is able to give numerical solutions with sufficient accuracy [28].

Unlike the complete-wave HLLC upwind scheme which restores the contact discontinuities by modifying the wave structures of the incomplete-wave HLL scheme but fails to preserve its robustness against the shock anomalies in calculations of multidimensional strong shock waves [5], the proposed FORCE-BVD centred scheme restores the contact discontinuities by using an algebraic method and thus is capable of preserving the shock stability of the original FORCE centred scheme. In what follows, the shock stability analysis of the FORCE-BVD scheme is conducted to demonstrate its robustness.

3.2. Shock stability analysis

The domain $[0,1]\times[0,1]$ is covered by a 25×25 uniform Cartesian mesh and a steady standing shock is located on interfaces shared by cells in the 12th and 13th columns. The upstream

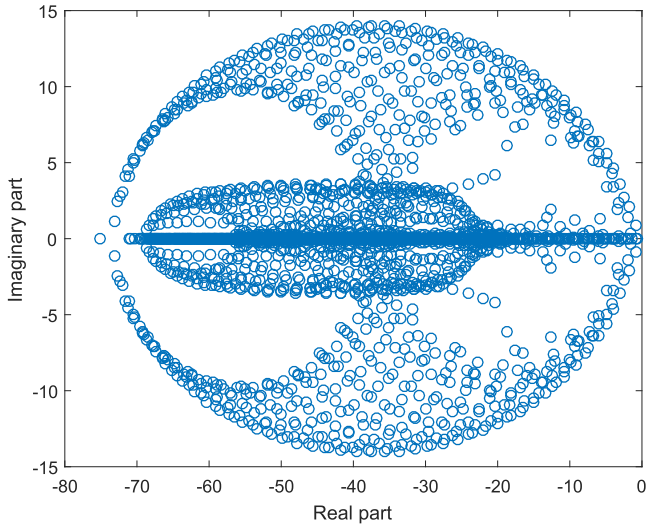

(a) FORCE, $\max(\mathrm{Re}(\lambda)) = -0.6988$

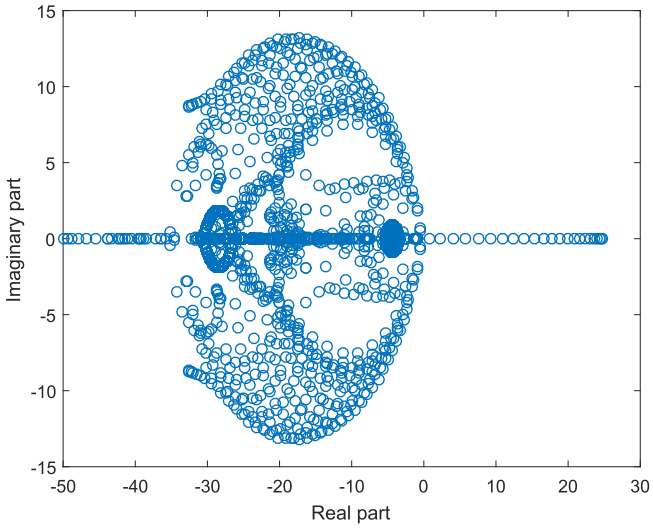

(b) HLLC, $\max(\mathrm{Re}(\lambda)) = 24.7545$

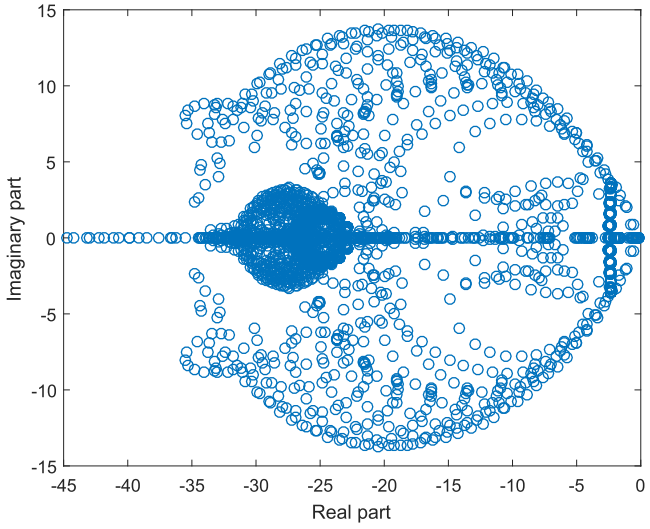

(c) FORCE-BVD, $\max(\mathrm{Re}(\lambda)) = -0.1140$

Fig. 1. Distribution of eigenvalues of the stability matrix **S** for different numerical schemes.

condition of the shock is given as

$$\overline{\mathbf{U}}_{(0)} = \left(1, 1, 0, \frac{1}{\gamma(\gamma-1)M^2} + \frac{1}{2}\right)^{\mathrm{T}} \tag{3.8}$$

and the downstream condition determined by the Rankine-Hugoniot relations is

$$\begin{aligned} &\overline{\mathbf{U}}_{(1)} = \left(g(M), 1, 0, \tfrac{h(M)}{\gamma(\gamma-1)M^2} + \tfrac{1}{2g(M)}\right)^{\mathrm{T}}, \\ &g(M) = \left(\tfrac{2}{\gamma+1}\tfrac{1}{M^2} + \tfrac{\gamma-1}{\gamma+1}\right)^{-1}, \\ &h(M) = \tfrac{2\gamma}{\gamma+1}M^2 - \tfrac{\gamma-1}{\gamma+1}, \end{aligned} \tag{3.9}$$

where M is the Mach number and is set to 10 in the current analysis. The upstream and downstream conditions are fixed at the left and right boundaries respectively whilst the periodic conditions are used for the top and bottom boundaries.

The flow field evolved from the initial conditions (3.8) and (3.9) can be written as

$$\overline{\mathbf{U}}_m = \mathbf{U}_m^0 + \delta\mathbf{U}_m, \tag{3.10}$$

where $\mathbf{U}_m^0$ and $\delta\mathbf{U}_m$ denote the steady mean value and the error respectively, m represents the global index of a cell. For the stability analysis of a steady field, the temporal evolution of errors in the entire flow field needs to be investigated. In the present analysis, we avoid introducing any artificial perturbations into the flow field and just study the evolution of numerical errors brought by a specific numerical method. For it, a matrix-based stability analysis procedure originally put forward by Dumbser et al [30] is carried out.

After the linearization procedure, the numerical flux through an interface shared by cells with global indices m and k can be expressed as

$$\Psi_{mk}(\overline{\mathbf{U}}_m, \overline{\mathbf{U}}_k) = \Psi_{mk}(\mathbf{U}_m^0, \mathbf{U}_k^0) + \frac{\partial\Psi_{mk}}{\partial\overline{\mathbf{U}}_m}\cdot\delta\mathbf{U}_m + \frac{\partial\Psi_{mk}}{\partial\overline{\mathbf{U}}_k}\cdot\delta\mathbf{U}_k. \tag{3.11}$$

Substituting (3.11) into (2.5), we can obtain the temporal evolution model of the numerical error

$$\frac{d(\delta \mathbf{U}_m)}{dt} = -\frac{1}{|\Omega_m|}\sum_{\Gamma_{mk}\subset\partial\Omega_m}|\Gamma_{mk}|\left[\frac{\partial \Psi_{mk}}{\partial \overline{\mathbf{U}}_m}\cdot\delta\mathbf{U}_m + \frac{\partial \Psi_{mk}}{\partial \overline{\mathbf{U}}_k}\cdot\delta\mathbf{U}_k\right], \tag{3.12}$$

where $|\Omega_m|$ denotes the area of the cell with index m and $|\Gamma_{mk}|$ is the length of cell interface Γ_{mk}. From (3.12), the evolutionary system of numerical errors in the entire flow field can be expressed as

$$\frac{d}{dt}\begin{bmatrix}\delta\mathbf{U}_1\\ \vdots \\ \delta\mathbf{U}_N\end{bmatrix} = \mathbf{S}\begin{bmatrix}\delta\mathbf{U}_1\\ \vdots \\ \delta\mathbf{U}_N\end{bmatrix}, \tag{3.13}$$

where $N = 25\times 25$ is the total number of cells and $\mathbf{S}$ denotes a stability matrix that will vary depending on numerical schemes. The solution of (3.13) is

$$\begin{bmatrix}\delta\mathbf{U}_1\\ \vdots \\ \delta\mathbf{U}_N\end{bmatrix}(t) = e^{\mathbf{S}t}\begin{bmatrix}\delta\mathbf{U}_1\\ \vdots \\ \delta\mathbf{U}_N\end{bmatrix}_{t=0} \tag{3.14}$$

which is bounded so long as

$$\max\left(\mathrm{Re}(\lambda)\right) \leqslant 0, \tag{3.15}$$

where $\mathrm{Re}(\lambda)$ represent the real parts of eigenvalues of $\mathbf{S}$.

The dimension of the stability matrix $\mathbf{S}$ is 2500 and the standard algorithm in MATLAB is used to obtain its eigenvalues. Fig. 1 shows all eigenvalues of the stability matrix $\mathbf{S}$ in a complex plane. The complete-wave HLLC upwind scheme, which is well known to be afflicted with the shock instability, has multiple eigenvalues with positive real parts that will result in a destabilized solution. The eigenvalues of the FORCE and the proposed FORCE-BVD centred schemes, however, are always with negative real parts that imply a stable pattern. The result of stability analysis shows the better shock stability of the FORCE-BVD centred scheme over the HLLC upwind scheme, which is fully demonstrated by the results of numerical experiments in Section 4 as well.

4. Numerical results

A series of one-dimensional and two-dimensional benchmark test problems are calculated in this section to evaluate the performance of the proposed FORCE-BVD centred scheme, including its accuracy for contact discontinuities and robustness against the shock anomalies, and a systematic comparison with the original FORCE scheme, the complete-wave HLLC upwind scheme and the RTV flux splitting scheme [25] is also made. Unless otherwise specified, we use the second-order accuracy to discrete the time and space, which is achieved by using the second-order SSP Runge-Kutta method [31] and the second-order MUSCL scheme [29].

4.1. Isolated contact wave

The computational domain [0,1] is divided into 100 uniform cells and the initial condition is given by

$$(\rho_0, u_0, p_0) = \begin{cases}(1.4, 0.1, 1.0), & 0 \leqslant x \leqslant 0.5,\\ (1.0, 0.1, 1.0), & 0.5 < x \leqslant 1.\end{cases} \tag{4.1}$$

This is an isolated contact wave propagating at Mach 0.1. Fig. 2 shows the density distribution of the original FORCE scheme, HLLC scheme, the RTV flux splitting scheme as well as the proposed FORCE-BVD scheme at $t = 2$. It can be clearly observed that the proposed FORCE-BVD centred scheme captures the sharp jump of the density field with the least dissipation. This test case fully demonstrates that the proposed FORCE-BVD centred scheme is superior to the original FORCE centred scheme, the RTV flux splitting scheme and even the complete-wave HLLC upwind scheme in the capability of capturing contact discontinuity.

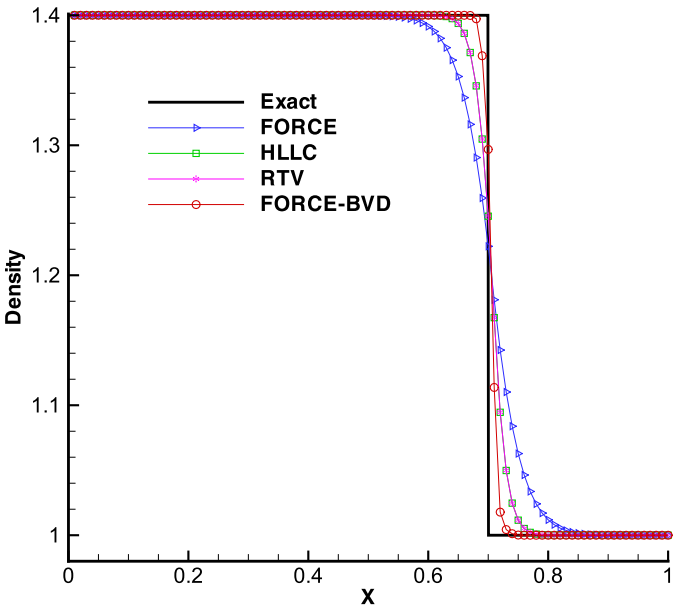

Fig. 2. Distribution of density for an isolated contact wave propagating at Mach 0.1.

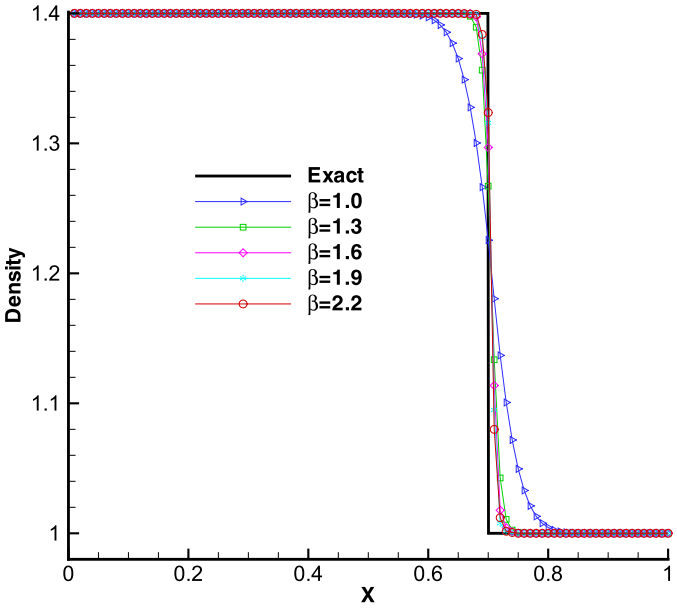

Fig. 3. Density distribution of the FORCE-BVD scheme with different β.

Fig. 3 shows the results of the proposed FORCE-BVD centred scheme with different values of β. It can be seen that steep jumps are obtained by all the values of β except for $\beta = 1.0$. In order to evaluate quantitatively, the thickness measurement of a discontinuity proposed in [32] is introduced:

$$\delta_{thickness} = \frac{\rho_{jump}}{\Delta x}\cdot\frac{1}{\max\left(\left|\frac{\delta\rho}{\delta x}\right|\right)} = \frac{\rho_{jump}}{\max(|\rho_i - \rho_{i-1}|)}, \tag{4.2}$$

where $\rho_{jump} = 0.4$ for this test case. As shown in Table 1, the thickness of discontinuity decreases with the increase of β. A larger β gives a sharper interface but, as shown in Subsection 4.7, tends

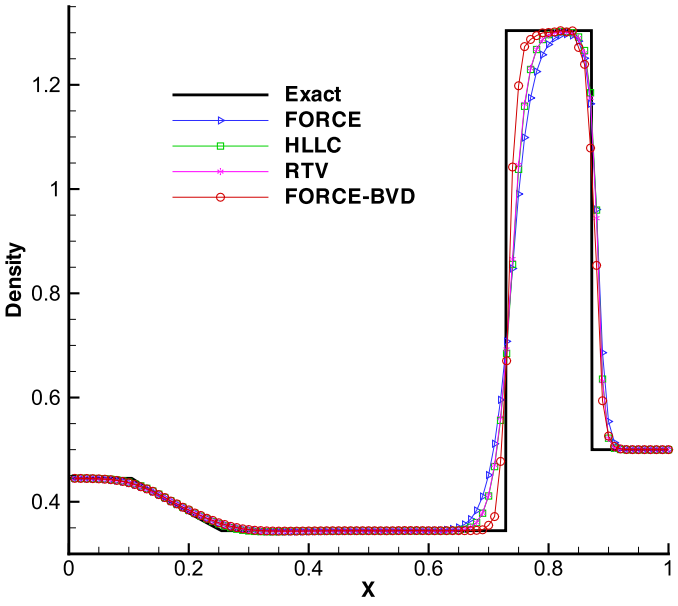

Fig. 4. Distribution of density for the Lax problem.

Table 1
Comparison of discontinuity thickness for different β.

	$\beta = 1.0$	$\beta = 1.3$	$\beta = 1.6$	$\beta = 1.9$	$\beta = 2.2$
$\delta_{thickness}$	8.8891	2.9914	2.1841	1.8099	1.6410

to wrinkle an interface parallel to the velocity direction [28]. It is found that a β ranging from 1.2 to 2.0 is able to give a sharp but less wrinkled interface. In this paper, we choose an ad hoc $\beta = 1.6$ for all numerical tests.

4.2. Lax problem

The Lax problem is calculated to examine the ability of the proposed FORCE-BVD centred scheme to capture the relatively strong shock wave [33]. The computational domain [0,1] is divided into 100 uniform cells and the initial condition is given by

$$(\rho_0, u_0, p_0) = \begin{cases} (0.445, 0.698, 3.528), & 0 \leqslant x \leqslant 0.5, \\ (0.5, 0, 0.571), & 0.5 < x \leqslant 1. \end{cases} \tag{4.3}$$

The initial condition involves with a relatively strong right traveling shock, a right traveling contact discontinuity and a left traveling expansion wave. Fig. 4 shows the density distribution of the original FORCE scheme, the HLLC scheme, the RTV flux splitting scheme as well as the proposed FORCE-BVD centred scheme at $t = 0.15$. It can be clearly observed that the resolution of all four numerical schemes for expansion wave and shock wave is almost identical whilst the proposed FORCE-BVD centred scheme can capture the contact discontinuity with less dissipation than the other three numerical schemes.

4.3. 1D blast wave problem

The computational domain [0,1] is divided into 500 uniform cells and the initial condition is given by

$$(\rho_0, u_0, p_0) = \begin{cases} (1.0, 0.0, 1000), & 0 \leqslant x \leqslant 0.1, \\ (1.0, 0.0, 0.01), & 0.1 < x \leqslant 0.9, \\ (1.0, 0.0, 100), & 0.9 < x \leqslant 1. \end{cases} \tag{4.4}$$

The reflective boundary conditions are imposed at the left and right sides. The initial condition involves with the collision of two strong shock waves and a complicated wave structure is formed with the interaction of these two shock waves. Fig. 5 shows the density distribution of four numerical schemes at $t = 0.038$. A zoomed plot in the region [0.5,0.64] is also given to make a more detailed comparison. It can be clearly seen that the proposed FORCE-BVD centred scheme performs best in this test case and captures the discontinuities with less dissipation than the other three schemes.

4.4. Shu-Osher problem

This test case is aimed at investigating the spectral and shock-capturing capability of a given numerical scheme [34]. The computational domain $[-5, 5]$ is divided into 1000 uniform cells and the

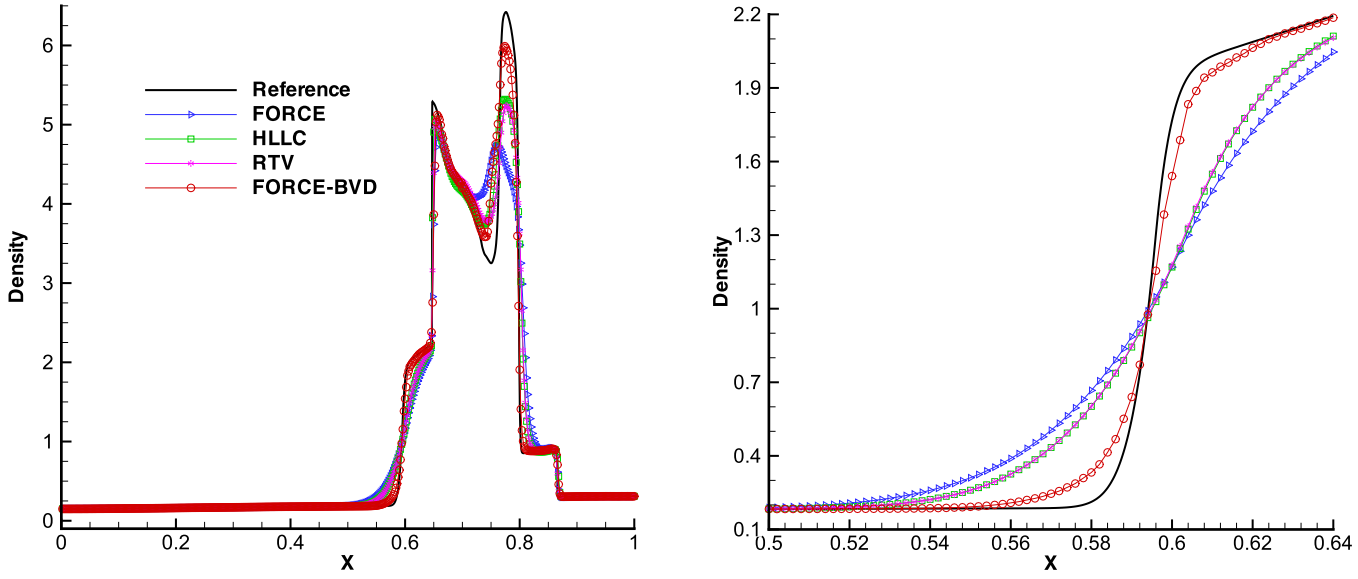

(a) Entire view (b) Enlargements

Fig. 5. Distribution of density for the 1D blast wave problem.

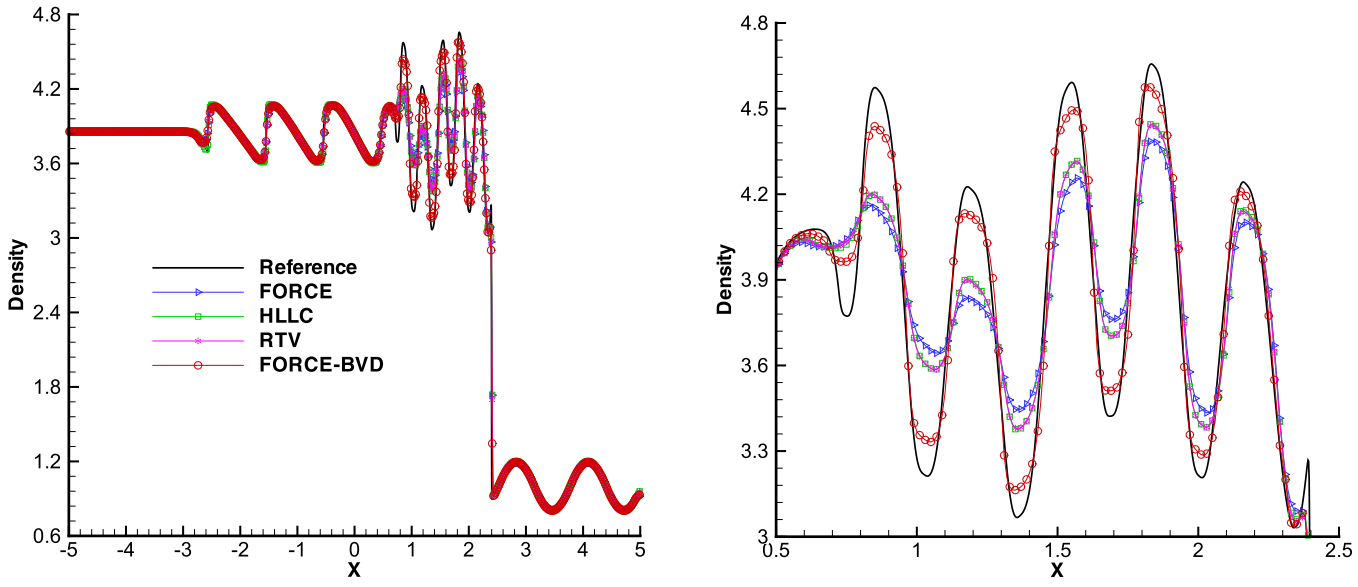

(a) Entire view (b) Enlargements

Fig. 6. Distribution of density for the Shu-Osher problem.

initial condition is given by

$$(\rho_0, u_0, p_0) = \begin{cases} (27/7, 4\sqrt{35}/9, 31/3), & -5 \leqslant x \leqslant -4, \\ (1 + 0.2\sin(5x), 0, 1), & -4 < x \leqslant 5. \end{cases} \tag{4.5}$$

The initial condition involves with the interaction of a sine entropy wave with a Mach 3 right traveling shock wave [35]. Fig. 6 shows the density distribution of four numerical schemes at $t = 1.8$. A zoomed plot in the region [0.5,2.5] is also given to make a more detailed comparison. It can be clearly observed that the proposed FORCE-BVD centred scheme can capture the high-frequency waves more accurately than the original FORCE centred scheme, the complete-wave HLLC upwind scheme and the RTV flux splitting scheme.

4.5. 2D explosion problem

The 2D explosion problem [36] which is an extension of 1D Sod's shock tube problem is calculated to test the capability of the proposed FORCE-BVD scheme for capturing various types of waves. The computational domain $[-1, 1] \times [-1, 1]$ is divided into a 201×201 uniform mesh and the initial condition is given by

$$(\rho_0, u_0, v_0, p_0) = \begin{cases} (1, 0, 0, 1), & x^2 + y^2 < 0.4^2, \\ (0.125, 0, 0, 0.1), & x^2 + y^2 \geqslant 0.4^2. \end{cases} \tag{4.6}$$

The computational final time is $t = 0.25$. At this time, the solution consists of a circular shock wave traveling outwards, a circular contact surface following the shock and a circular rarefaction travelling towards the centre [36]. Fig. 7 shows the density distribution along the radial line at $y = 0$. It can be observed that the proposed FORCE-BVD centred scheme is able to capture all types of waves accurately, especially for the contact discontinuity.

4.6. 2D Riemann problem

Next we consider a 2D Riemann problem which is proposed and analyzed extensively in [37]. The computational domain $[0, 1] \times [0, 1]$ is divided into a 1600×1600 uniform Cartesian mesh

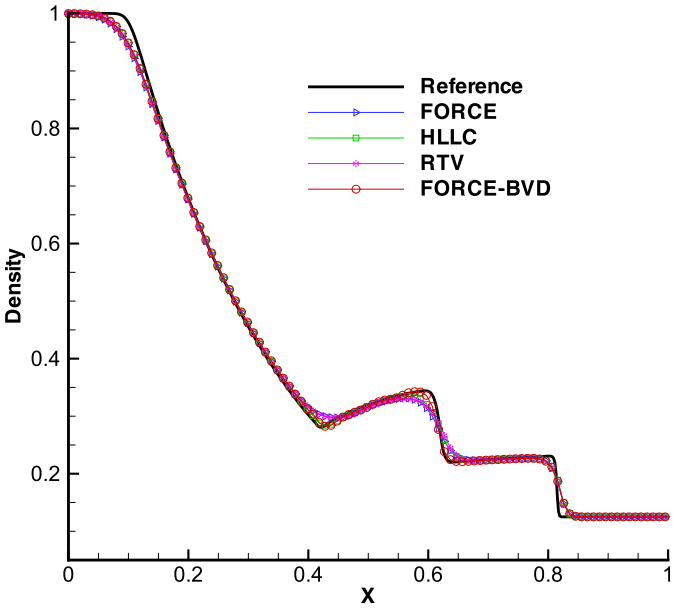

Fig. 7. Density distribution along the radial line for the 2D explosion problem.

and the initial condition is given by

$$(\rho_0, u_0, v_0, p_0) = \begin{cases} (1.0, 0.75, -0.5, 1.0), & x \geqslant 0.5,\ y \geqslant 0.5, \\ (2.0, 0.75, 0.5, 1.0), & x < 0.5,\ y \geqslant 0.5, \\ (1.0, -0.75, 0.5, 1.0), & x < 0.5,\ y < 0.5, \\ (3.0, -0.75, -0.5, 1.0), & x \geqslant 0.5,\ y < 0.5. \end{cases} \tag{4.7}$$

The initial condition involves with four contact discontinuities and four shear layers will be formed due to interactions of these contact discontinuities. Although the flow problem considered here is inviscid, the viscosity inherent in the numerical scheme is capable of triggering the shear instability, i.e. the Kelvin-Helmholtz instability. Since the capability of capturing contact discontinuities as well as the shear waves is critical to resolve the small-scale vorti-

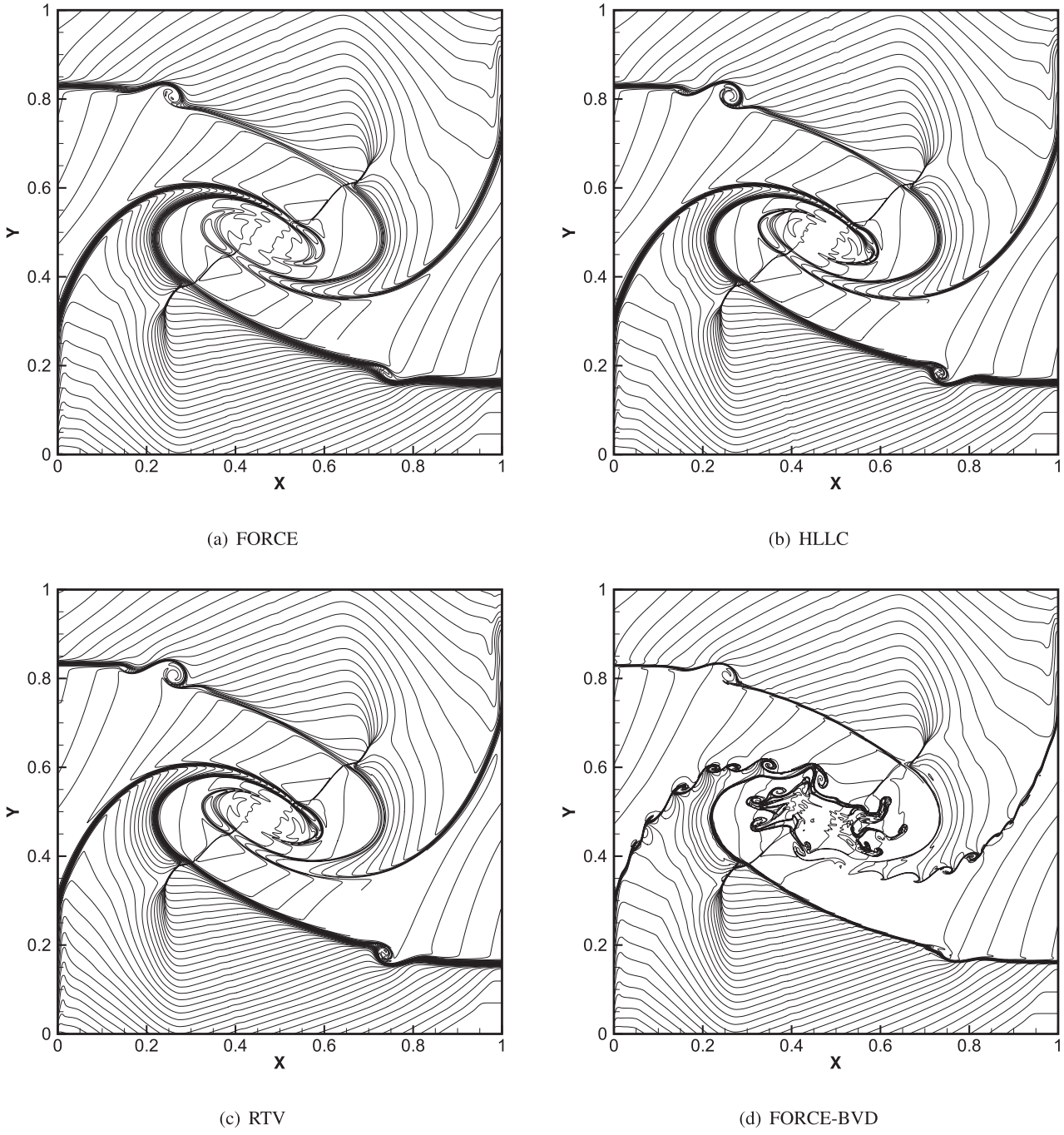

(a) FORCE (b) HLLC

(c) RTV (d) FORCE-BVD

Fig. 8. Density contours of the 2D Riemann problem.

cal structures created by the Kelvin-Helmholtz instability [38], the 2D Riemann problem is a very suitable numerical example to verify the accuracy of a given numerical scheme. Fig. 8 shows the density contours of four numerical schemes at $t = 0.8$. It can be clearly observed that the proposed FORCE-BVD centred scheme can not only resolve the shear layers more accurately but also capture the visible vortical structures caused by the Kelvin-Helmholtz instability whilst the original FORCE centred scheme, the complete-wave HLLC upwind scheme and the RTV flux splitting scheme obtain solutions with more dissipation.

4.7. 2D interface only problem

The two-dimensional interface only problem proposed in [39] is calculated to compare the ability of different numerical schemes to capture contact surfaces. The computational domain $[0, 1] \times [0, 1]$ is divided into a 100×100 uniform Cartesian mesh and the initial condition is given by

$$(\rho_0, u_0, v_0, p_0) = \begin{cases} (2, 1, 1, 1), & \sqrt{(x-0.2)^2 + (y-0.2)^2} < 0.01, \\ (1, 1, 1, 1), & \sqrt{(x-0.2)^2 + (y-0.2)^2} \geqslant 0.01. \end{cases} \tag{4.8}$$

The corresponding exact solution at $t = 0.3$ is as follows

$$(\rho_0, u_0, v_0, p_0) = \begin{cases} (2, 1, 1, 1), & \sqrt{(x-0.5)^2 + (y-0.5)^2} < 0.01, \\ (1, 1, 1, 1), & \sqrt{(x-0.5)^2 + (y-0.5)^2} \geqslant 0.01. \end{cases} \tag{4.9}$$

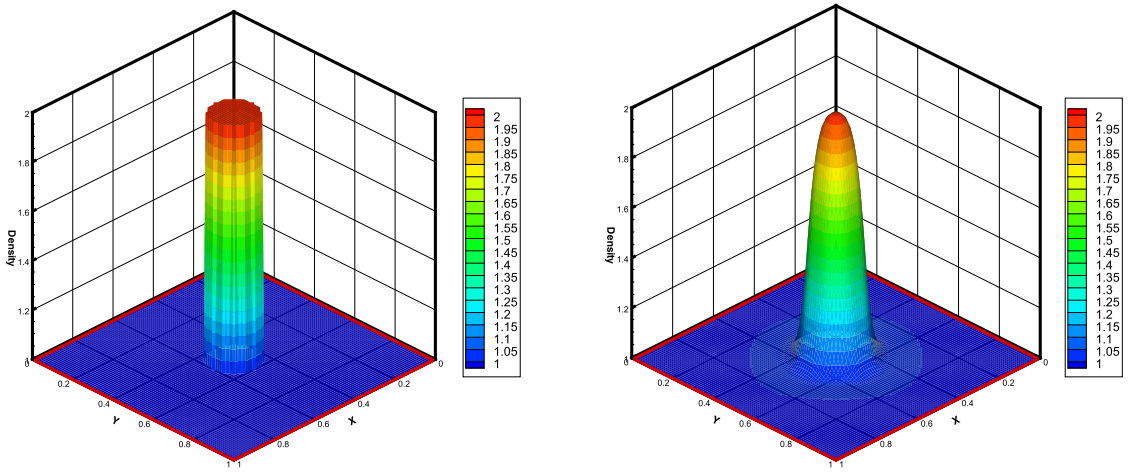

(a) Exact solution (b) FORCE

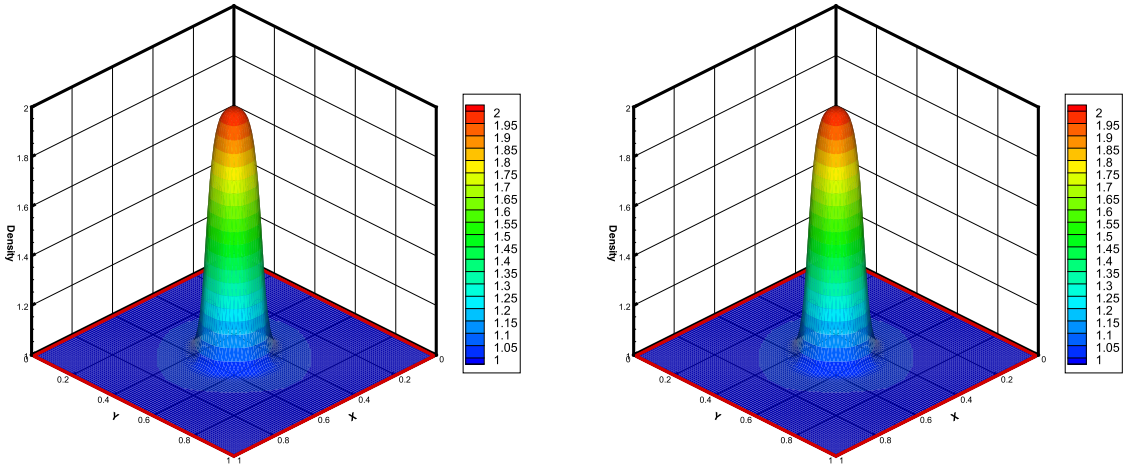

(c) HLLC (d) RTV

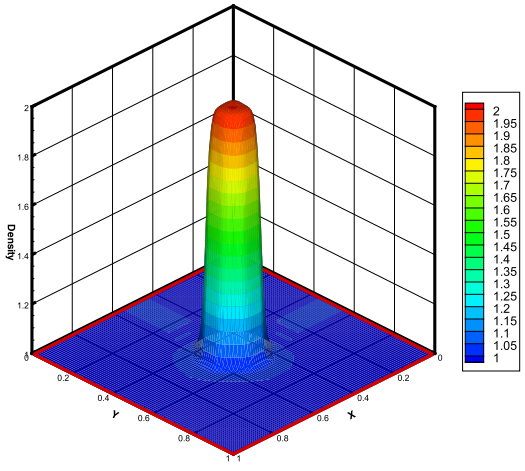

(e) FORCE-BVD

Fig. 9. Surface plots of the density for the 2D interface only problem.

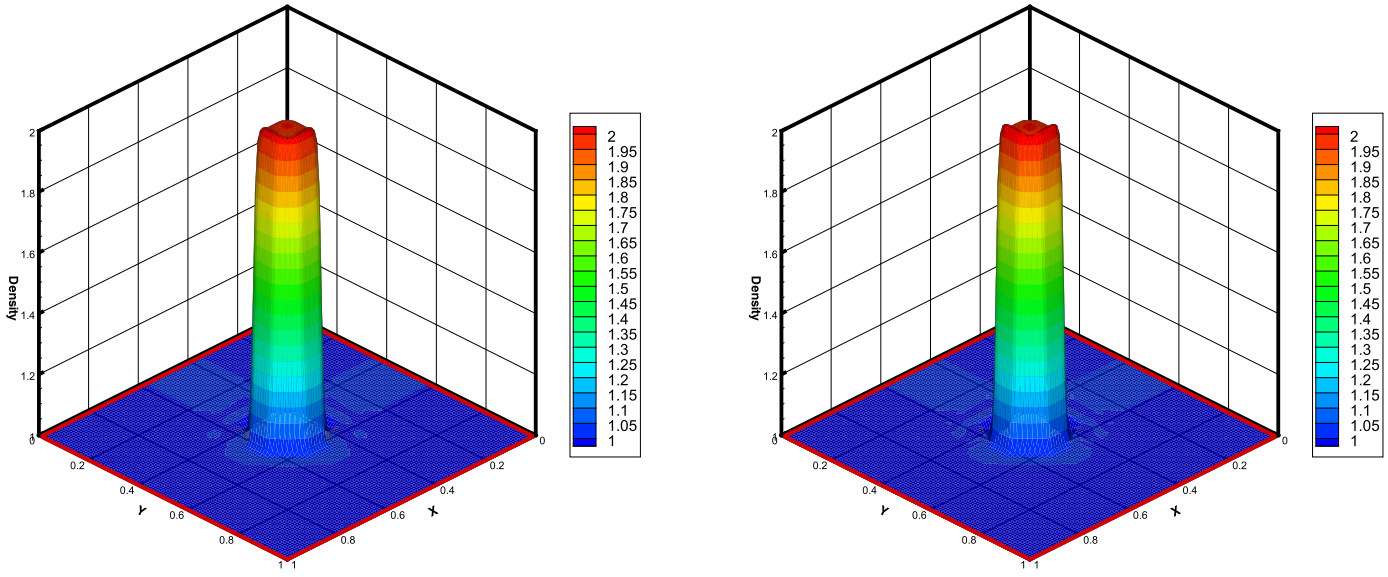

(a) FORCE-BVD, $\beta = 3.0$ (b) FORCE-BVD, $\beta = 3.6$

Fig. 10. Surface plots of the density calculated by the FORCE-BVD scheme with different β.

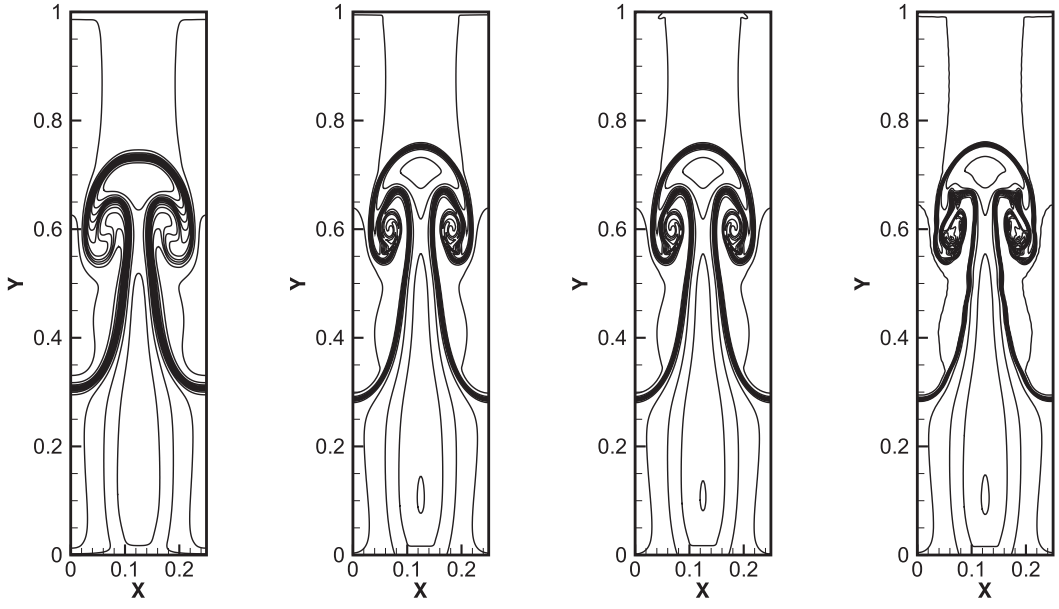

(a) FORCE (b) HLLC (c) RTV (d) FORCE-BVD

Fig. 11. Density contours of the Rayleigh-Taylor instability problem.

Fig. 9 shows the exact solution and four numerical solutions at $t = 0.3$. It can be clearly observed that the proposed FORCE-BVD centred scheme resolves the contact surface more sharply than the original FORCE centred scheme, the HLLC upwind scheme and the RTV flux splitting scheme. Fig. 10 shows the results of the FORCE-BVD scheme with larger values of β. A larger β gives a sharper interface but tends to wrinkle an interface parallel to the velocity direction. It is found that a moderate β ranging from 1.2 to 2.0 is able to give a satisfactory solution.

4.8. Rayleigh-Taylor instability problem

Initially, two fluids with different densities are separated by $y = 0.5$ and the Rayleigh-Taylor instability will develop when an acceleration is directed from the heavier fluid to the lighter one [27,40]. The computational domain $[0, 0.25] \times [0, 1]$ is partitioned into a 120×480 uniform mesh and the initial condition is given by

$$(\rho_0, u_0, v_0, p_0) = \begin{cases} (2, 0, -0.025a_0 \cos(8\pi x), 1 + 2y), & 0 \leqslant y \leqslant 0.5, \\ (1, 0, -0.025a_0 \cos(8\pi x), 1.5 + y), & 0.5 < y \leqslant 1, \end{cases} \tag{4.10}$$

where $a_0 = \sqrt{\gamma p_0/\rho_0}$ is the sound speed and the specific heat ratio $\gamma = 5/3$ in this case. Reflective conditions are used at the left and right boundaries. We assign $(\rho, u, v, p) = (1, 0, 0, 2.5)$ on the top boundary and $(\rho, u, v, p) = (2, 0, 0, 1)$ on the bottom boundary. The gravitational effect is also considered by adding a source

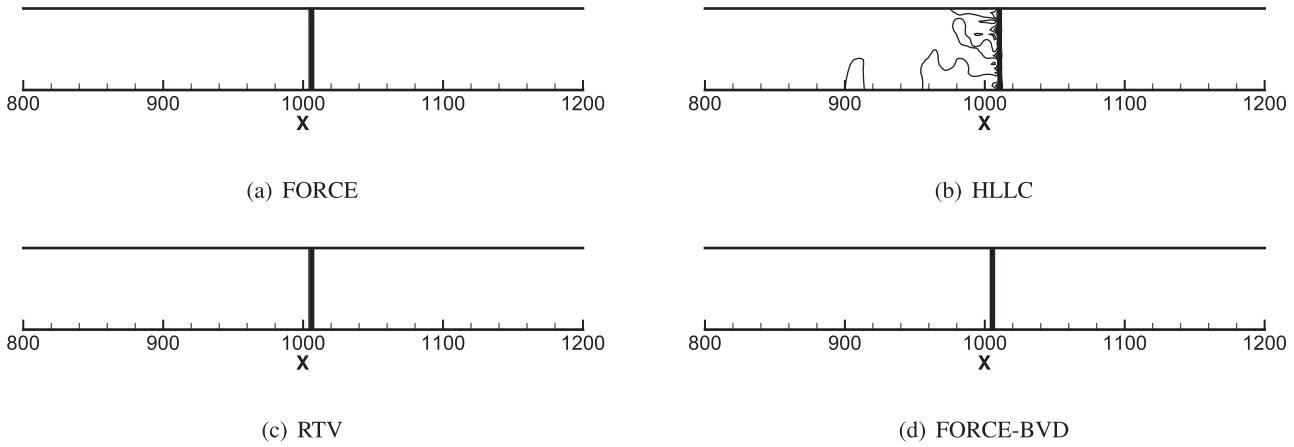

(a) FORCE (b) HLLC

(c) RTV (d) FORCE-BVD

Fig. 12. Density contours of the random numerical noise problem.

term $\mathbf{S} = (0, 0, \rho, \rho v)^{\mathrm{T}}$ into the right-hand side of the system (2.1). Fig. 11 shows the density contours of four numerical schemes at $t = 1.95$. It can be clearly observed that the proposed FORCE-BVD centred scheme is capable of resolving the sharper material interfaces and capturing more vortical structures on the interfaces as compared to the original FORCE centred scheme, the HLLC upwind scheme and the RTV flux splitting scheme, indicating that it is less dissipative than the other three numerical schemes.

4.9. Random numerical noise problem

Riemann solvers that can capture contact discontinuities accurately usually suffer from the shock anomalies, such as the most common carbuncle phenomenon, in solving multidimensional flow problems involving strong shock waves. The proposed FORCE-BVD scheme restores the contact waves by using an algebraic method and does not modify the wave structures of the original FORCE scheme. Therefore, it preserves the shock stability of the original FORCE scheme very well. A Mach 10 planar normal shock problem is calculated here to demonstrate the robustness of the proposed FORCE-BVD scheme.

The Mach 10 normal shock is initially located at $x = 5$ and travels from left to right along a duct that covers a domain $[0, 1200] \times [0, 20]$. The initial condition is given by

$$(\rho_0, u_0, v_0, p_0) = \begin{cases} (1.4, 0, 0, 1), & x > 5, \\ (8, 8.25, 0, 116.5), & x \leqslant 5, \end{cases} \tag{4.11}$$

In the planar normal shock instability problem proposed by Quirk [41], the instability is triggered by the small disturbance of the y-directional grid centerline. Here we leave the gridline undisturbed but introduce the following random numerical noises into the pre-shock state of the initial flow field:

$$(\rho_0, u_0, v_0, p_0)_{i,j} = (1.4, 0, 0, 1) + (\beta_1, \beta_2, \beta_3, \beta_4)_{i,j} \cdot 10^{-6}, \tag{4.12}$$

where $\beta_k (k = 1, 2, 3, 4)$ are random numbers between -0.5 and 0.5.

Fig. 12 shows the density contours of four numerical schemes at $t = 100$. It can be clearly observed that the complete-wave HLLC upwind scheme suffers from the visible shock instability whilst the original FORCE centred scheme, the RTV flux splitting scheme and the proposed FORCE-BVD centred scheme obtain a stable solution without any non-physical behavior. The maximal deviation of y-velocity shown in Fig. 13 also demonstrates the robustness of the proposed FORCE-BVD scheme. The maximal y-velocity of the HLLC scheme grows rapidly from the initial order of 10^{-6} to order of 10^{0} whilst it stays at the initial order of 10^{-6} if we choose

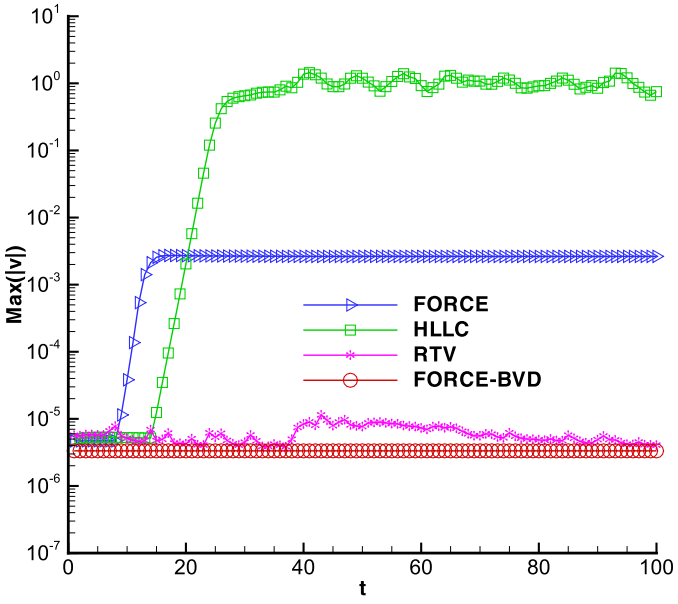

Fig. 13. The maximal deviation of y-velocity for the random numerical noise problem.

the FORCE-BVD flux. It is worth noting that although the original FORCE scheme and the RTV flux splitting scheme give a clean shock front without any oscillation, their corresponding maximal y-velocity has risen to the order of 10^{-3} and 10^{-5}, respectively.

4.10. Sedov blast wave problem

The Sedov blast wave problem involving high pressure ratio and strong shock waves is considered here to examine the robustness of the proposed FORCE-BVD scheme. The computational domain $[0, 2.4] \times [0, 2.4]$ is divided into a 480×480 uniform mesh and the initial condition of the entire flow field is given by $(\rho_0, u_0, v_0, p_0) = (1.0,\ 0.0,\ 0.0,\ 10^{-10})$ except that the pressure value at the center of the domain is $3.5 \cdot 10^5$. Reflective conditions are imposed at all four boundaries. Fig. 14 shows the density contours of four numerical schemes at $t = 0.1$. It can be clearly observed that the complete-wave HLLC upwind scheme exhibits four visible carbuncles at places where the shock front is aligned with the grid-line whilst the original FORCE centred scheme, the RTV flux splitting scheme and the proposed FORCE-BVD centred

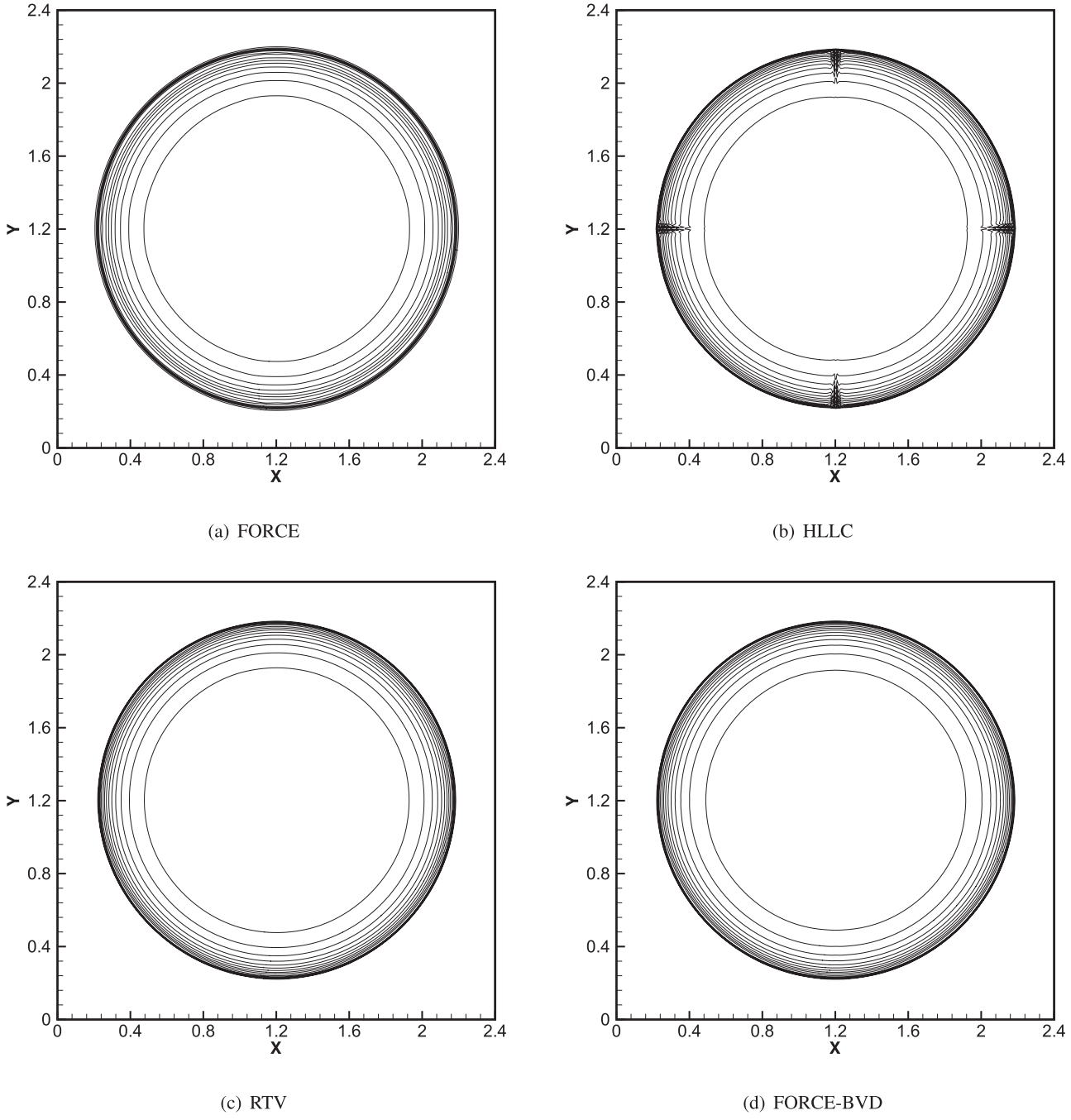

(a) FORCE (b) HLLC

(c) RTV (d) FORCE-BVD

Fig. 14. Density contours of the Sedov blast wave problem.

scheme are all capable of obtaining a stable shock front without any oscillation.

4.11. Shock diffraction problem

The supersonic corner flow problem, which involves the diffraction of a Mach 5.09 normal shock over a 90° corner, is studied here to examine the robustness of the proposed scheme. The computational domain $[0, 1] \times [0, 1]$ is partitioned into a 400×400 uniform mesh and the location of the corner is $(x, y) = (0.05, 0.625)$. The pre-shock condition on the right side of the shock is given by $(\rho_0, u_0, v_0, p_0) = (1.4, 0, 0, 1)$. The post shock condition is imposed at the inlet boundary whilst the outlet boundary is set to zero gradient for all primitive variables. The boundary condition at the top changes with time to consider the shock's motion. The zero gradient condition for all primitive variables is used at the bottom boundary and the left boundary below the corner adopts the reflective condition. Fig. 15 shows the density contours of four numerical schemes at $t = 0.1561$. It can be clearly observed that the visible oscillations appearing on the top of the normal shock badly contaminate the solution of the HLLC scheme whilst all of the original FORCE scheme, the RTV flux splitting scheme and the proposed FORCE-BVD scheme obtain a stable shock configuration without any oscillation. It is worth noting that the normal shock captured by the RTV scheme slightly contaminates the upper boundary layer. However, the solution calculated by the proposed FORCE-BVD scheme does not encounter it.

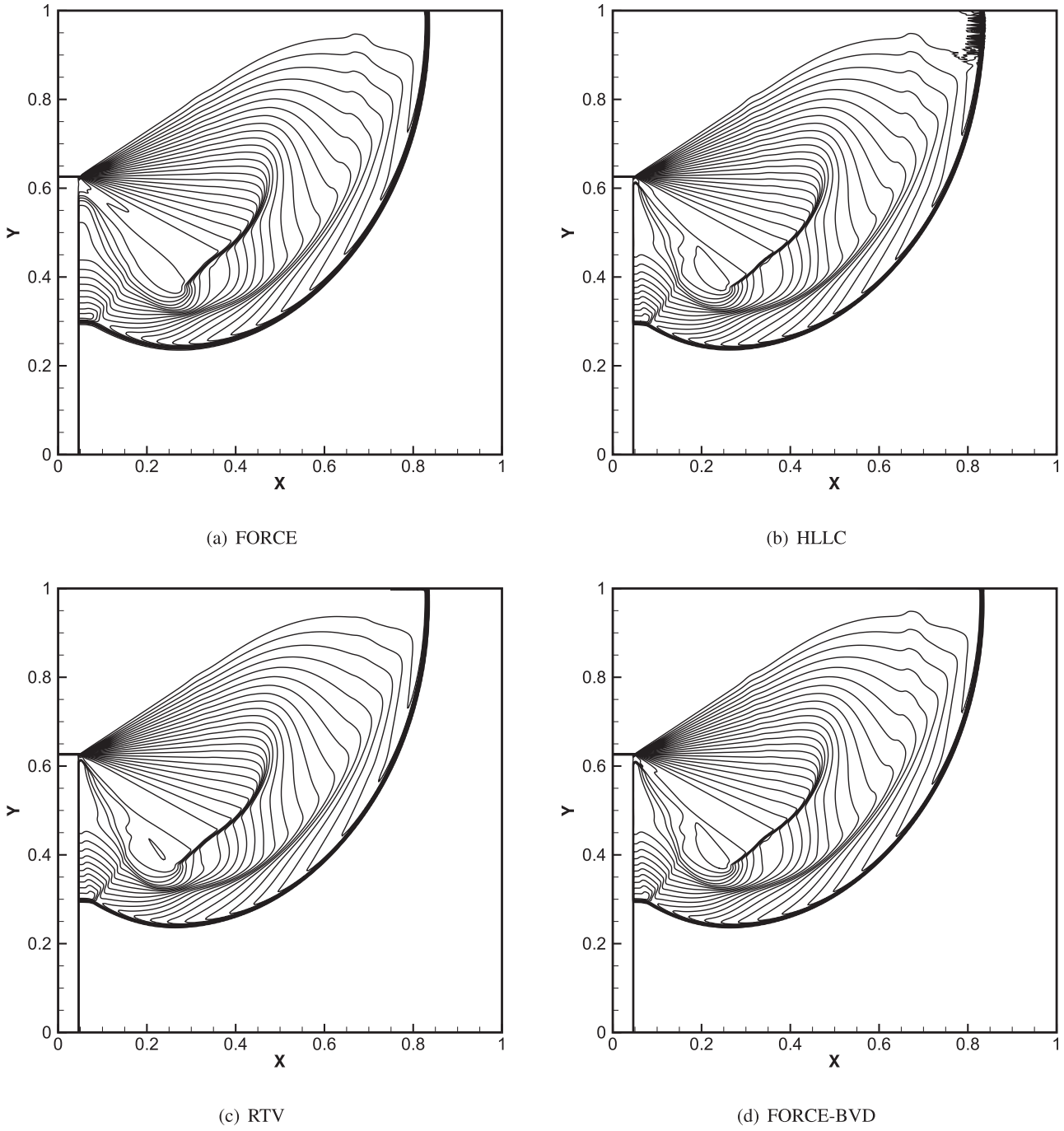

(a) FORCE (b) HLLC

(c) RTV (d) FORCE-BVD

Fig. 15. Density contours of the shock diffraction problem.

4.12. Effect of the order of accuracy

It should be noted that the use of BVD algorithm resembles the use of high order schemes, i.e. one wants to reduce the jump term in the numerical flux so that the numerical dissipation is reduced. The above numerical experiments show that the proposed FORCE-BVD scheme has higher contact resolution than the other numerical schemes when using the second-order MUSCL reconstruction. In order to evaluate the proposed scheme comprehensively, we discuss the effect of the order of accuracy in this subsection and the fifth-order variant of the weighted essentially non-oscillatory method [42], i.e. WENO5, is considered here.

We first consider the isolated contact wave problem described in Subsection 4.1. For this simple 1D Riemann problem, the proposed FORCE-BVD scheme combined with the second-order MUSCL reconstruction, as shown in Table 2, gives a steeper jump than the other three solvers combined with the fifth-order WENO reconstruction. In order to avoid the effect of temporal discretization on numerical results, the third-order Runge-Kutta scheme [31] is adopted in this subsection.

Next, the problem of two-dimensional turbulent flow driven by the Kelvin-Helmholtz instability is calculated to compare the performance of different numerical schemes. The computational domain $[-0.5, 0.5] \times [-0.5, 0.5]$ is divided into a 500×500 uniform

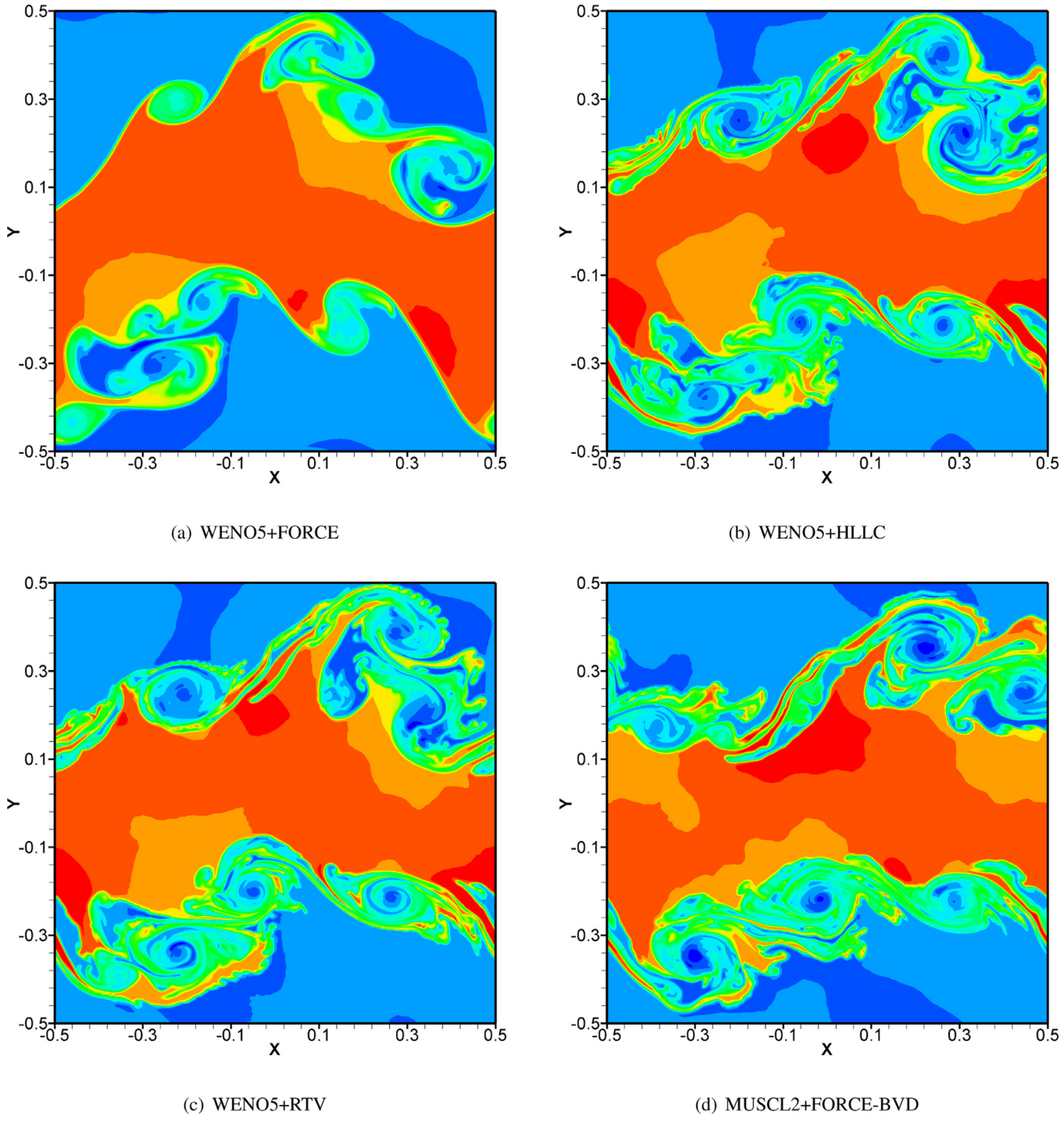

(a) WENO5+FORCE (b) WENO5+HLLC

(c) WENO5+RTV (d) MUSCL2+FORCE-BVD

Fig. 16. Density contour plots at time $t = 2$ for the Kelvin-Helmholtz instability problem.

Table 2
Comparison of discontinuity thickness for the isolated contact wave problem.

	WENO5+FORCE	WENO5+HLLC	WENO5+RTV	MUSCL2+FORCE-BVD
$\delta_{thickness}$	5.2343	3.4080	3.4057	2.1841

mesh and the initial condition is given by

$$(\rho_0, u_0, v_0, p_0) = \begin{cases} (2, -0.5, 0.01\sin(2\pi x), 2.5), & |y| \leqslant 0.25, \\ (1, 0.5, 0.01\sin(2\pi x), 2.5), & |y| > 0.25. \end{cases} \tag{4.13}$$

Periodic boundary conditions are used in both directions. Due to the Kelvin-Helmholtz instability, small vortexes at the sharp density interface will be generated and become bigger through a vortex merging mechanism [43]. These vortexes evolve freely and interact with each other to form a two-dimensional turbulence regime [43].

Table 3
Total CPU time (in hours) of different schemes for the Kelvin-Helmholtz instability problem.

Scheme	WENO5+FORCE	WENO5+HLLC	WENO5+RTV	MUSCL2+FORCE-BVD
CPU time	5.0117	6.1209	6.8357	3.6853

As shown in Fig. 16, the FORCE centred scheme combined with the fifth-order WENO reconstruction produces a more dissipative result which yields less filamentation processes while the proposed FORCE-BVD scheme combined with the second-order MUSCL reconstruction gives a solution that is comparable to solutions calculated from the HLLC and RTV schemes combined with the fifth-order WENO reconstruction. The total CPU time (on an Intel Core i5-5200U with 2.20GHz processor) for calculating this Kelvin-Helmholtz instability problem at time $t = 2$ is shown in Table 3 from which it can be concluded that the proposed FORCE-BVD scheme is more computationally efficient than the other three schemes.

5. Conclusions

In this work, a FORCE-type centred scheme accurate for contact discontinuities is proposed and it has been applied to the calculation of compressible Euler flows. Using a jump-like THINC function to reconstruct the density values on both sides of the cell interface, the missing contact discontinuity of the original FORCE centred scheme is restored. The resolution of the proposed scheme for contact discontinuities is further improved by using the BVD (Boundary Variation Diminishing) algorithm to minimize the density difference in the numerical dissipation term of the FORCE centred scheme. Numerical results of a series of 1D and 2D test problems fully demonstrate that the proposed scheme can capture the contact discontinuities more sharply than the complete-wave HLLC upwind scheme. In addition, as the contact is restored with an algebraic method, the proposed scheme preserves the shock stability of the original FORCE scheme very well. In calculations of multi-dimensional flow problems involving strong shock waves, the proposed FORCE-BVD scheme can effectively suppress the shock instabilities which usually afflict the contact-capturing upwind schemes (such as Roe and HLLC). The proposed scheme is simple and easy to implement and can be easily extended to higher order accuracy by combining with the existing polynomial reconstruction methods (e.g. MUSCL and WENO). Future work will focus on the applications of the proposed centred scheme to other conservative and non-conservative systems.

Declaration of Competing Interest

The authors declare that they have no known competing financial interests or personal relationships that could have appeared to influence the work reported in this paper.

CRediT authorship contribution statement

Lijun Hu: Conceptualization, Methodology, Writing - original draft. **Li Yuan:** Writing - review & editing.

Acknowledgements

The constructive comments of the anonymous reviewers are gratefully acknowledged. This work was supported by the National Natural Science Foundation of China (91641107, 91852116), the Science and Technology Plan Project of Hunan Province (Hunan Provincial Key Laboratory of Intelligent Information Processing and Application, 2016TP1020), the Application-oriented Characterized Disciplines, Double First-Class University Project of Hunan Province (Xiangjiaotong [2018]469).

References

[1] Toro EF, Hidalgo A, Dumbser M. FORCE schemes on unstructured meshes i: conservative hyperbolic systems. J Comput Phys 2009;228:3368–89.
[2] Chen GQ, Toro EF. Centered difference schemes for nonlinear hyperbolic equations. J Hyberbolic Differ Equ 2004;1:531–66.
[3] Harten A, Lax PD, van Leer B. On upstream differencing and godunov-type schemes for hyperbolic conservation laws. SIAM Rev 1983;25:35–61.
[4] Einfeldt B. On godunov-type methods for gas dynamics. SIAM J Numer Anal 1988;25:294–318.
[5] Mandal JC, Panwar V. Robust HLL-type riemann solver capable of resolving contact discontinuity. Comput Fluids 2012;63:148–64.
[6] Simon S, Mandal JC. A cure for numerical shock instability in HLLC riemann solver using antidiffusion control. Comput Fluids 2018;174:144–66.
[7] Roe PL. Approximate riemann solvers, parameter vectors, and difference schemes. J Comput Phys 1981;43:357–72.
[8] Osher S, Solomon F. Upwind difference schemes for hyperbolic systems of conservation laws. Math Comput 1982;38:339–74.
[9] Einfeldt B, Munz CD, Roe PL, Sjögreen B. On godunov-type methods near low densities. J Comput Phys 1991;92:273–95.
[10] Toro EF, Spruce M, Speares W. Restoration of the contact surface in the HLL-riemann solver. Shock Waves 1994;4:25–34.
[11] Lax PD. Weak solutions of nonlinear hyperbolic equations and their numerical computation. Comm Pure Appl Math 1954;7:159–93.
[12] Nessyahu H, Tadmor E. Non-oscillatory central differencing for hyperbolic conservation laws. J Comput Phys 1990;87:408–63.
[13] Bianco F, Puppo G, Russo G. High order central schemes for hyperbolic systems of conservation laws. SIAM J Sci Comput 1999;21:294–322.
[14] Levy D, Puppo G, Russo G. A fourth order central WENO scheme for multidimensional hyperbolic systems of conservation laws. SIAM J Sci Comput 2002;24:480–506.
[15] Kurganov A, Petrova G. Central-upwind schemes on triangular grids for hyperbolic systems of conservation laws,. Numer Methods Partial Differ Eq 2005;21:536–52.
[16] Qiu JX, Shu CW. On the construction, comparison, and local characteristic decomposition for high-order central WENO schemes. J Comput Phys 2002;183:187–209.
[17] Toro EF, Billet SJ. Centered TVD schemes for hyperbolic conservation laws. IMA J Numer Anal 2000;20:44–79.
[18] Dumbser M, Hidalgo A, Castro M, Parés C, Toro EF. FORCE Schemes on unstructured meshes II: non-conservative hyperbolic systems. Comput Methods Appl Mech Engrg 2010;199:625–47.
[19] Boscheri W, Dumbser M, Righetti M. FORCE schemes on moving unstructured meshes for hyperbolic systems. Comput Math Appl 2019;78:362–80.
[20] Canestrelli A, Toro EF. Restoration of the contact surface in FORCE-type centred schemes I: homogeneous two-dimensional shallow water equations. Adv Water Resour 2012;47:88–99.
[21] Kurganov A, Lin C. On the reduction of numerical dissipation in central-upwind schemes. Commun Comput Phys 2007;2:141–63.
[22] Stecca G, Siviglia A, Toro EF. Upwind-biased FORCE schemes with applications to free-surface shallow flows. J Comput Phys 2010;229:6362–80.
[23] Canestrelli A, Toro EF. Restoration of the contact surface in FORCE-type centred schemes II: non-conservative one- and two-layer two-dimensional shallow water equations. Adv Water Resour 2012;47:76–87.
[24] Sun Z, Inaba S, Xiao F. Boundary variation diminishing (BVD) reconstruction: a new approach to improve godunov schemes. J Comput Phys 2016;322:309–25.
[25] Hu L, Feng S. A robust and contact preserving flux splitting scheme for compressible flows. Commun Nonlinear Sci Numer Simulat 2020;93:105502.
[26] Deng X, Xie B, Loubère R, Shimizu Y, Xiao F. Limiter-free discontinuity-capturing scheme for compressible gas dynamics with reactive fronts. Comput Fluids 2018;171:1–14.
[27] Deng X, Boivin P, Xiao F. A new formulation for two-wave Riemann solver accurate at contact interfaces. Phys Fluids 2019;31:046102.
[28] Xiao F, Honma Y, Kono T. A simple algebraic interface capturing scheme using hyperbolic tangent function. Int J Numer Methods Fluids 2005;48:1023–40.
[29] van Leer B. Towards the ultimate conservative difference scheme. v. a second-order sequel to godunov's method. J Comput Phys 1979;32:101–36.
[30] Dumbser M, Moschetta JM, Gressier J. A matrix stability analysis of the carbuncle phenomenon. J Comput Phys 2004;197:647–70.
[31] Gottlieb S, Shu CW, Tadmor E. Strong stability-preserving high-order time discretization methods. SIAM Rev 2001;43:89–112.
[32] Nonomura T, Kitamura K, Fujii K. A simple interface sharpening technique with a hyperbolic tangent function applied to compressible two-fluid modeling. J Comput Phys 2014;258:95–117.

[33] Shu CW, Osher S. Efficient implementation of essentially non-oscillatory shock--capturing schemes. J Comput Phys 1988;77:439–71.
[34] Kumar R, Chandrashekar P. Efficient seventh order WENO schemes of adaptive order for hyperbolic conservation laws. Comput Fluids 2019;190:49–76.
[35] Jiang GS, Shu CW. Efficient implementation of weighted ENO schemes. J Comput Phys 1996;126:202–28.
[36] Toro EF. Riemann solvers and numerical methods for fluid dynamics: A Practical introduction. Berlin, Heidelberg: Springer-Verlag; 2009.
[37] Schulz-Rinne CW. Classification of the Riemann problem for two-dimensional gas dynamics. SIAM J Math Anal 1993;24:76–88.
[38] Dumbser M, Zanotti O, Loubère R, Diot S. A posteriori subcell limiting of the discontinuous galerkin finite element method for hyperbolic conservation laws. J Comput Phys 2014;278:47–75.
[39] Chen Y, Jiang S. Modified kinetic flux vector splitting schemes for compressible flows. J Comput Phys 2009;228:3582–604.
[40] Wang Y, Du Y, Zhao K, Yuan L. A new 6th-order WENO scheme with modified stencils. Comput Fluids 2020;208:104625.
[41] Quirk JJ. A contribution to the great riemann solver debate. Int J Numer Methods Fluids 1994;18:555–74.
[42] Titarev VA, Toro EF. WENO schemes based on upwind and centred TVD fluxes. Comput Fluids 2005;34:705–20.
[43] San O, Kara K. Evaluation of Riemann flux solvers for WENO reconstruction schemes: Kelvin-helmholtz instability. Comput Fluids 2015;117:24–41.